Carbohydrate Polymers 201 (2018) 87–95

Contents lists available at ScienceDirect

Carbohydrate Polymers

journal homepage: www.elsevier.com/locate/carbpol

Cell interactions and cytotoxic studies of cellulose nanofibers from Curauá natural fibers

Sivoney Ferreira Souza[a,b,*], Marcos Mariano[b,c], Dennys Reis[d], Christiane Bertachini Lombello[e], Mariselma Ferreira[e], Mohini Sain[a]

[a] Center for Biocomposites and Biomaterials Processing, Faculty of Forestry, University of Toronto, 33 Willcocks St., Toronto, ON, M5S3B3, Canada
[b] Actual: Brazilian National Laboratory of Nanotechnology at Brazilian National Center of Research in Energy and Materials, Campinas, SP, 13083-970, Brazil
[c] Institute of Chemistry, State University of Campinas - UNICAMP, Campinas, SP, 13083-970, Brazil
[d] Institute of Physics, University of Sao Paulo - USP, São Paulo, SP, 05508-090, Brazil
[e] Universidade Federal do ABC, Centro de Ciências Naturais e Humanas, Av. dos Estados, 5001, Santo André, SP, 09210-580, Brazil

ARTICLE INFO

Keywords:
Nanocellulose
Nanofibrillated cellulose
Microfibrillated cellulose
Tensile strength
Rheology
Biocompatibility

ABSTRACT

Cellulose nanofibers (CNF) were isolated from Curauá fibers (*Ananas erectifolius* L. *B. Smith*) through a mechanical grinder preceded by mild chemical treatment. Morphology and surface characteristics of the fibers were followed until it reaches the nanoscale as long and flexible nanofibers. In aqueous suspensions, SAXS techniques revealed that such nanofibers present a twisted ribbon structure while rheological measurements demonstrate its high viscosity and a thixotropic behavior. These characteristics suggests the potential application of CNF in biomedical field, which, in turn, stimulates the toxicological studies of such materials. The obtained materials do not show any sign of cytotoxicity by direct or indirect assays for cell viability and cell morphology using *Vero* cells. Moreover, during the adhesion test, the cells demonstrated higher affinity to the CNF surface. It can be related to its surface properties and its obtaining conditions, which did not use any hazardous chemicals.

1. Introduction

Nanocellulose has been one of the most explored nanomaterials over the last years. It corresponds to a generical term to specify cellulose particles with dimensions in nanoscale. Basically, there are two main materials that can be obtained from lignocellulosic sources: cellulose nanocrystals (CNC) and cellulose nanofibers (CNF). CNC are rigid rod shape particles usually produced by strong acid hydrolysis (De France, Hoare, & Cranston, 2017). Meanwhile, CNF are longer and flexible, being also called as nanofibrillated cellulose (NFC) and normally obtained by mechanical shear (Charreau, Foresti, & Vazquez, 2012). This popularity arises from a combination of abundant sources, low cost and optimal physical properties, since these materials present a high aspect ratio allied to flexibility and toughness.

It's first successfully trials as driver of outstanding reinforcement phase in nanocomposites resulted in an expansion in the number of potential applications of such materials. Some examples are given by its utilization to improve permeability control(Bardet et al., 2015), nanocomposites (Dufresne, 2017), rheological properties (Nazari, Kumar, Bousfield, & Toivakka, 2016), hydrogels (De France et al., 2017), preparation of special papers (Castro et al., 2018), aerogels (Mariano, Bernardes, & Strauss, 2018) and even support for conductive paints and batteries (El Baradai et al., 2016; Hoeng, Denneulin, & Bras, 2016).

Nowadays, the processing techniques to isolate and characterize these nanoparticles are already well established and an exponential grown in the number of different sources can be verified in literature (Cherian et al., 2011). The great aspect of this expansion is to provide biomass valorization, transforming residues from agriculture in nanoparticles with potential to present commercial value through a low cost process (Novo, Bras, Garcia, Belgacem, & Curvelo, 2015). Considering the abundance of biomass, the characteristics can significantly vary for each vegetal source, for instance, the size of nanocrystalline domains, crystallinity index, mechanical resistance (Jonoobi et al., 2015). The optimization of these properties and identification of the best source for each aimed application is a laborious work that is still progressing. Its importance lies in the need of solid knowledge of the surface properties and toxicity of these materials that needs to be enlightened.

Very recent studies shows nanocellulose-based systems are being tested for some biomedical applications as composites to bone replacement, artificial skins and scaffolds to tissue and cells growing (Jorfi & Foster, 2015; Smyth et al., 2017). These applications are based on nanocellulose non-toxicity. However, actual research state is still not

* Corresponding author.
E-mail address: sivoney.souza@lnnano.cnpem.br (S.F. Souza).

https://doi.org/10.1016/j.carbpol.2018.08.056
Received 25 May 2018; Received in revised form 11 August 2018; Accepted 13 August 2018
Available online 15 August 2018

totally conclusive, and many steps are required before clinical trials. Additional toxicity tests and *in vivo* studies (with three different animal models), are just some examples. Indeed, the toxicity of such materials depends on source, experimental procedures (chemical, mechanical or enzymatic), functionalization and aimed final application. In this scenario, there are only a few studies about cytotoxicity and adhesion tests of cellulose nanofibers obtained by mechanical shear from the grinder (Supermasscoloider Masuko®) from Curauá fibers.

Here, Curauá fibers were chosen to be studied mainly due to their high amount of cellulose and its unique superior mechanical properties that can be an advantage in preparation of several bio-based materials such as nanocellulose in general (Souza et al., 2010; Souza et al., 2014; Oliveira de Castro, Frollini, Ruvolo-Filho, & Dufresne, 2015). CNF from Curauá fibers was produced using mild reaction conditions and a smaller number of cycles through the mechanical grinder. Further physical-chemical characterization of the obtained CNF was extensively studied together with small angle X-ray scattering (SAXS) analysis, which gave insights on the native structure of nanofibrillated cellulose. The obtained CNF presented good mechanical properties, as a solid membrane, studied by stress strain tests, and as hydrogels studied by rheology. Both properties show that the obtained material can be used to prepare different scaffolds for biomedical applications Therefore, the toxicological behavior of cellulose nanofibers from Curauá fibers were investigated with fibroblasts cells (*Vero* cells as the cell lineage) by the direct and indirect contact assay. Later, the adhesion test on the CNF surface were also evaluated with same cells.

2. Materials and methods

2.1. Cellulose nanofibers isolation

Curauá leaf fibers (*Ananas erectifolius*), originally from São Paulo State, were obtained from UNESP – Sao Paulo State University, Rural Engineering Department, where they are kept in a genetic bank. The fibers were milled and passed through a sieve with 4 mm mesh, dried at 60 °C overnight to remove moisture, and then treated with 0.05 N HCl solution for 2 h at 70 °C. To the resulting suspension was added NH_4OH solution until reaching pH 9.5. Later, the pulping process was done using 4% NaOH solution (1:10) at 70 °C for 2 h. Then, the fibers were bleached with 8.6 mL of acetic acid and 9 g of $NaOCl_2$ per 100 g of dried pulp and 800 mL of water, and the reaction was carried out for 40 min at ca. 70 °C. The bleached fibers were processed mechanically 12 times using the commercial grinder (Supermasscolloider MKZA 10–15 J, Masuko Sangyo Co., Japan®).

2.2. Samples characterization

2.2.1. Thermal properties

It was determined by thermogravimetric analysisusing a TGA Q500 V6 Build 203 instrument under nitrogen environment, with heating from 25 °C to 600 °C at 10 °C min^{-1}.

2.2.2. FTIR

The specimens were dispersed in KBr and determined using FTIR with a Bruker-Tensor 27 spectrum, with 32 scans in the range between 4000 and 400 cm^{-1}.

2.2.3. XRD

The X-Ray diffractions spectra were obtained with a Philips Analytical X-ray PW 1830 generator (45 kV, 100 mA) equipped with Cu Kα radiation (λ = 0.1541 nm), in the 10–40° 2θ range and step size of 0.02° in 2θ. The relative crystallinity index was calculated using the method proposed by Segal, Creely, Martin, and Conrad (1959) as described by Ghali, Msahli, Zidi, and Sakli, (2009):

$$C.I. = \frac{I_{002} - I_{am}}{I_{002}} * 100$$

where C.I. is the relative crystallinity index, I_{002} is the maximum diffraction intensity at the main peak around 2θ = 22.5°, and I_{am} is the intensity of the amorphous peak around 18°.

2.2.4. Microscopies (SEM, STEM and AFM)

Scanning electron microscopy (SEM) images were performed using Jeol Scanning Electron Microscope – JSM-6610 LV. Samples were placed on the carbon tape for the analysis. CNF suspension was analyzed under environmental transmission electronic microscopy (STEM) using FEI-Quanta FEG 250 equipment. For the STEM analysis, it was dropped 10 μL of CNF suspension on the concentration of 5 mg L^{-1} on the copper grids with 400 mesh and dried at room temperature. For atomic force microscope (AFM) analysis, CNF suspension was sonicated for 5 min in the concentration of 5 mg L^{-1}. Later, 10 μL was dropped in mica and dried environmentally. The AFM analysis were performed at a Park NX10 equipment using tapping mode. The particles diameter was calculated by using CNF height (Z axis), obtained by the difference between the CNF height and substrate after drawing a line through the sample to get a height profile. Around 100 measurements were performed.

2.2.5. Small-angle X-ray scattering (SAXS)

The analysis was performed using the SAXS1 beamline at LNLS, Brazilian Synchrotron Light Laboratory (CNPEM, Campinas, Brazil). The CNF suspension was loaded into liquid cell sample holders and sandwiched in-between mica windows. The data were collected at a photon energy of 8 keV (λ = 0.154 nm) using a Pilatus 300k detector, with a pixel size of 172 × 172 μm^2. The sample-to-detector distance was 1.2 m, covering a q-range from 0.12 to 4.5 nm^{-1}, where $q = 4\pi sin\theta/\lambda$ is the scattering vector modulus and 2θ is the scattering angle. Twenty frames of 30 s each were recorded; if no radiation damage was noticed, then the frames were averaged, and the background was subtracted from the data. As the sample and the corresponding scattering pattern are isotropic, frame integration was performed resulting in a curve of scattering intensity I as a function of scattering vector modulus q, $I = I(q)$. Curve analysis was performed by model fitting using our own Python software. It uses the Levenberg-Marquardt non-linear least square algorithm as implemented in Scipy 0.19.0 Optimization and Root Finding module (Jones, Oliphant, & Peterson, 2014).

2.2.6. Rheological behavior

Continuous flow and viscoelastic properties of CNF suspensions were analyzed on a Kinexus rotation rheometer equipped with parallel plate geometry (20 mm diameter) and a sample gap of 0.010 mm at the temperature of 25 °C, in triplicate. Measurements were performed in a plate-plate (20 mm) geometry. In a typical experiment, small amplitude oscillatory shear (SAOS) experiments were performed at a constant shear stress of 1 Pa at frequencies from 0.1 to 10 Hz at 20 °C. Oscillatory analyses were started by the conduction of a stress sweep, to determine the viscoelastic region of the sample.

2.3. Biological assays

Cytotoxicity assays of CNF were performed using a Vero cell lineage according to ISO 10993-5 recommendations (CCIAL 057) and their fibroblast-like features. The cellular response, induced by CNF, was investigated using indirect test and direct contact tests, while the scaffold potential was observed with the cell adhesion assay. The Vero cells were cultured with HAMF10 medium, 10% fetal bovine serum, and 1% antibiotics at pH 7.4. The cells were maintained at 37 °C and 5% CO_2.

2.3.1. Indirect cytotoxicity

The CNF membranes, produced before for tensile strength, were cut

into pieces of 1 cm^2 and sterilized in alcohol 70% for 12 h and exposed to ultraviolet light for 30 min (Souza, Leao, Lombello, Sain, & Ferreira, 2017). Later, samples were incubated in 5 mL culture medium for 24 h to produce the CNF extracts. Cells were incubated for 24 h until confluence. Then, the culture medium was replaced by the CNF extracts. For negative control (CTL-), the culture medium was renewed and for positive control (CTL+), the culture medium was replaced by solution of 0.25% phenol. All incubations lasted 24 h. Then, the medium was removed and 10 μL of MTT (5 mg/mL) dissolved in phosphate buffer was added during 4 h. An aliquot of 50 μL of DMSO was added for 30 min. The absorbance was measured in an Elisa reader at 570 nm (Spectramax M5) and correlated with the calibration curve. The cells were also observed through phase contrast in the optical microscope AxioVert A1, Zeiss. For that, the adhered cells were fixed with glutaraldehyde 2.5% for 20 min, washed and stained with 0.15% toluidine blue for 30 min.

2.3.2. Direct contact assay

It was performed according to ISO 10993-5. CNF suspension was dried on a glass slide at 60 °C for 4 h, sterilized in autoclave for 30 min at 127 °C. Vero cells were seeded directly onto the CNF films and onto glass slide autoclaved for negative control (CTR-). All the samples were cultivated at ideal growing conditions for 24 h. Later, the culture medium was removed, and the cells were fixed with 2.5% glutaraldehyde solution in 0.05 M phosphate buffer (pH 7.4 supplemented with sucrose and calcium chloride) for 3 h. Inverted microscopy images were obtained from the cells before fixation. Thereafter, the glass slides were washed in 0.1 M phosphate buffer for 1 h and fixed in 1% osmium tetroxide for 1 h. The drying process consisted in specimen immersion for 30 min in ethanol solutions (70, 75, 80, 85, 90, 95 and 100%), and later acetone (100%). The dried cells were coated with a gold layer and the images were acquired using a scanning electron microscope JSM-6010LA, JEOL, at the Multiuser facility at UFABC (Federal University of ABC).

2.3.3. Adhesion test

CNF suspension were dried onto the 96-well plates for 2 h at 60 °C. Sterilization was performed with 70% ethylic alcohol for 2 h and UV light for 30 min. The backscattering was represented by the culture medium. Positive controls were prepared by seeding the cells directly onto the culture plate. For negative control the silicone membrane was used as non-adherent surface. 1×10^4 cells per well were incubated during 2 h. The entire volume of supernatant inside the wells was transferred to new wells to quantify the unbound cells. Therefore, the cells adhered on the surface of each material were indirectly calculated through the quantification of cells non-adhered and the initial cells seeded. This was performed by adding 100 μL of solution with 10 μL of MTT solution (5 mg/mL) dissolved in 90 μL sterile PBS per well to the supernatant containing culture medium and cells and incubated for 4 h. Then, 50 μL of DMSO were added in each well for 30 min. The absorbance was measured on an ELISA Plate Reader (Spectramax M5) at $\lambda = 570$ nm, which was correlated with a calibration curve. All the experiments were performed six times.

2.3.4. Statistical analyses

The absorbance readings were statistically evaluated using the software basis GraphPad Prism version 6.0 and Microsoft Excel. For comparison we used ANOVA (One Way), the Tukey test and the t-student, where values were considered significant when $p > 0.05$.

3. Results

3.1. Fibers processing and morphology

In general, methods described in the literature to obtain CNFs are based on two processing steps: (i) lignocellulosic materials receive chemical (or enzymatic) treatments aiming to isolate cellulose fibers, which is followed by (ii) a mechanical defibrillation of the same fibers. In first one, most common chemical methods normally involve TEMPO-oxidation prior to mechanical shearing (Nechyporchuk, Belgacem, & Pignon, 2014). Resultant oxidation degree of these fibers is determinant for the high efficiency of posterior defibrillation, which will be promoted by a supermasscolloider that mechanically disintegrate cellulose fibers until they reach the nanometric scale, releasing isolated nanoparticles called cellulose nanofibrils. The number of cycles can varies from 5 to 60, depending on the cellulose source and pre-treatment (Nechyporchuk et al., 2014; Nge, Lee, & Endo, 2013). Here, we were able to obtain a gel-like suspension of nanoparticles by direct application of the shearing after 12 cycles, escaping this chemical process with TEMPO. It suggests that Curauá fibers can be defibrillated with lower energy consumption compared to other fibers usually described in literature, probably due to the natural fiber morphology, composition and structural properties. It is very interesting considering that such fibers can present a high cellulose content (70.4 ± 2.3%) and allows the obtainment of CNF materials with very good mechanical properties, as discussed in the *Supporting information*.

The morphology of these fibers was followed along the applied treatments through SEM images (Fig. 1). Pristine Curauá fibers (CF) can be observed in Fig. 1A, with fibers revealing a rough surface material, probably owing to the presence of waxes and secondary compounds. These low molecular weight compounds were removed during bleaching processing, causing a drastic modification on fiber surface and dimensions in bleached fibers (BF). Fig. 1B present BF samples that becomes apparently more homogeneous after removal of secondary elements.

Due to the grinding features, which promotes shearing, particles size is reduced to nanoscale. A non-homogeneous particles distribution and its typical network structure was revealed by STEM. This feature is inherent from the mechanical process, where some fibers keep the diameter of the initial bleached fibers before grinding. However, as general rule, thin long and flexible nanoparticles are observed (Fig. 1C to F). The distribution of nanofiber´s cross section presented an average width of 6.4 ± 4.6 nm, as measured from the AFM images (Fig. 1E and F). The CNF lengths have dimensions of the order of micrometers, which provides a large aspect ratio for these nanoparticles (L/d relation). AFM images elucidate the three-dimensional organization of the nanofibrils network.

3.2. Physical-chemical characterizations

During processing, not only morphological but also chemical modifications of nanofibers are observed. The nature of such new surface characteristics is essential to understand its role during cell adhesions, for example. Fig. 2 presents FTIR, XRD, TG and DTG characterizations for pristine Curauá Fibers (CF), bleached (BF) and cellulose nanofibers (CNF). FTIR curves (Fig. 2A) for all samples have typical bands of cellulose structure, including −C−O− (1045 cm^{-1}), −C−H (2930 cm^{-1}) and −O−H (3350 cm^{-1}), which is broader at CNF due to its higher potential to absorb water from atmosphere (consequence of a higher surface area and free −OH groups, as indicated in TGA measurements in Fig. 2C). With progressive treatment of pristine fibers, the band at 1240 cm^{-1} (=C−O−C and =C−O) disappears after bleaching, indicating the decrease of lignin content. The same applies to bands at 1514 and 1735 cm^{-1} (ketone and acetyl C=O) assigned to hemicelluloses and lignin. The appearance of a well-defined band at 1645 cm^{-1} in CNF can be related to a slightly offset −O−H bending peak of absorbed water (normally observed at 1620 cm^{-1}).

Such chemical modification is also followed by a progressive modification of samples crystallinity (Fig. 2B). XRD patterns present characteristic peaks of cellulose type I allomorph. The peak at ca. 17.5 is attributed to the $1\underline{1}0$ and crystalline 110 plans, while the peak at larger angles is related to the 200 plan (Driemeier, Pimenta, & Rocha, 2011).

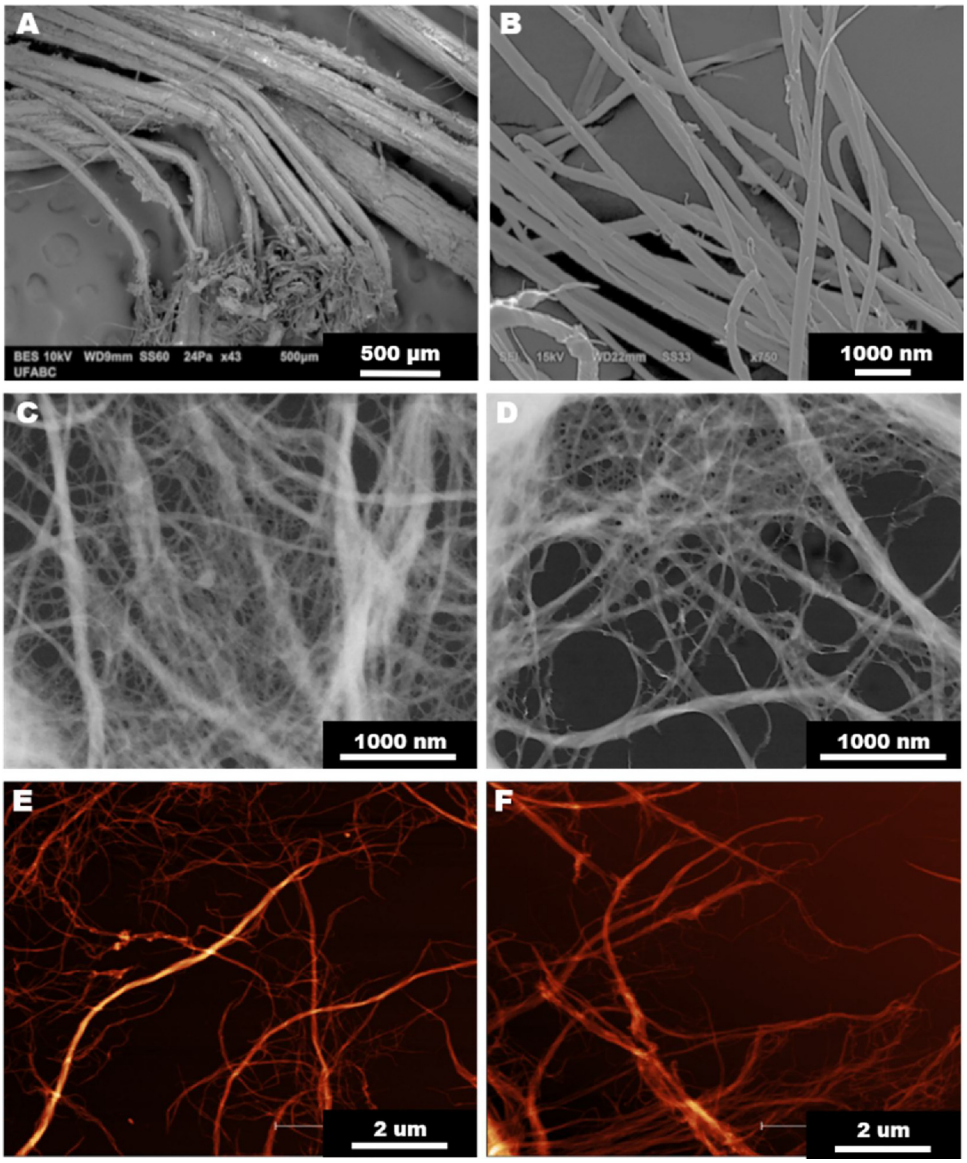

Fig. 1. SEM images of Curauá fibers (A) and bleached fibers (B). STEM images of cellulose nanofibers (C and D). AFM atomic force microscopy images of the final product CNF (E and F).

With processing, a small shift of 200 peak can be observed. It suggests a decrease in the distance between crystalline plans. Hence, bleaching and mechanical defibrillation caused the crystalline structure of the fibers to shrink during nanofibers isolation, and CNF have a more compact chain arrangement. As expected, one of the first consequences of natural fibers bleaching and defibrillation is a crystallinity increase owing to the removal of the amorphous lignin and hemicelluloses contents. Here, crystallinity content increased from 67 (CF) to 73.5% (BF) with bleaching. After twelve cycles through the grinder, CNF was isolated without rupture of the crystalline cellulose domains and sample crystallinity index was not affected. This stabilization of crystallinity is explained by the conservation amorphous regions. These results are similar to those of Zhao et al. (2013) for softwood nanofibers prepared by shear homogenization.

Higher surface area, chains packing, and cellulose content also modifies the thermal stability of the samples. Fig. 2C and 2D illustrates thermogravimetric and differential thermogravimetry results, respectively, for CF, BF and CNF samples. Obtained curves are characteristic of cellulosic materials. CNF presented a reduction on thermal stability, as can be seen by its lower maximum degradation temperature, than other samples (Fig. 2D). It can be related to the obtainment shear process, which promotes a breakage on micro cellulose structure and modifies fibers morphology, giving rise to high surface area particles (Iwamoto, Nakagaito, & Yano, 2007). CNF also present higher water content with a slightly later thermal degradation onset, which is followed by a higher residual content at 600 °C. Additional discussions can be found in the *Supporting information.*

3.3. CNF suspensions

The shape and rheology behavior of nanoparticles in aqueous suspensions were investigated through SAXS and rheological experiments, data are shown in Fig. 3A and B, respectively. CNF were modeled as a collection of non-interacting nanoparticles with shape of a twisted ribbon with rectangular cross section with semicircle ends, and infinite length, see the sketch in Fig. 3A. The proposed model is based on previous discussions (Lin & Dufresne, 2014; Mao et al., 2017) where the ribbon shape proposed by Su et al.(2014) was adopted for the CNF structure (Su, Burger, Hsiao, Chu, & IUCr, 2014). Similar fitting is due to the accessible q range of the used SAXS experimental setup, only the

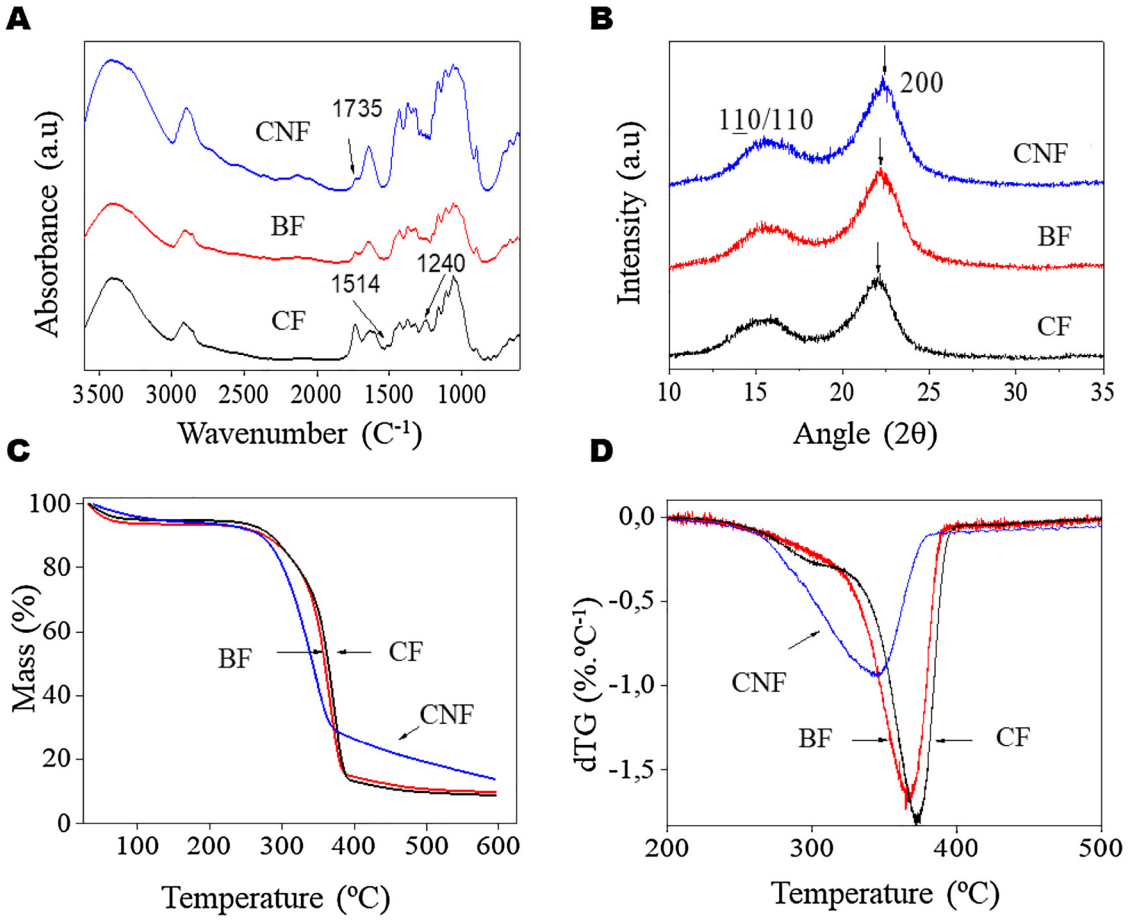

Fig. 2. A) FTIR spectra for all specimen, Curauá Fibers (CF), bleached (BF) and cellulose nanofibers (CNF). B) X-ray diffraction patterns. C) Thermal behavior and D) dTG curves.

ribbon's cross-section dimensions and respective dispersities could be obtained. The size polydispersity in a and b was included as gamma distributions. Such a model results in an analytical expression with six fit parameters: number average and standard deviation of the thickness (a,σ_a) and width (b,σ_b), a scaling factor, and a constant background term. The overall width of the ribbon's cross section is a + b (Su et al., 2014). The model fit to the experimental data is also presented in Fig. 3A, with the corresponding optimized values of the parameters in Table 1.

There is good agreement between the optimized model and the experimental data. The high aspect ratio of length to cross section's thickness and width is a reasonable hypothesis to our CNF samples as corroborated from the microscopy results. Also, the dimensions measured by SAXS presented low size polydispersities, although, the microscopy images didn't allow a clear distinction between the thickness and width of the fibers. The measured distribution parameters obtained

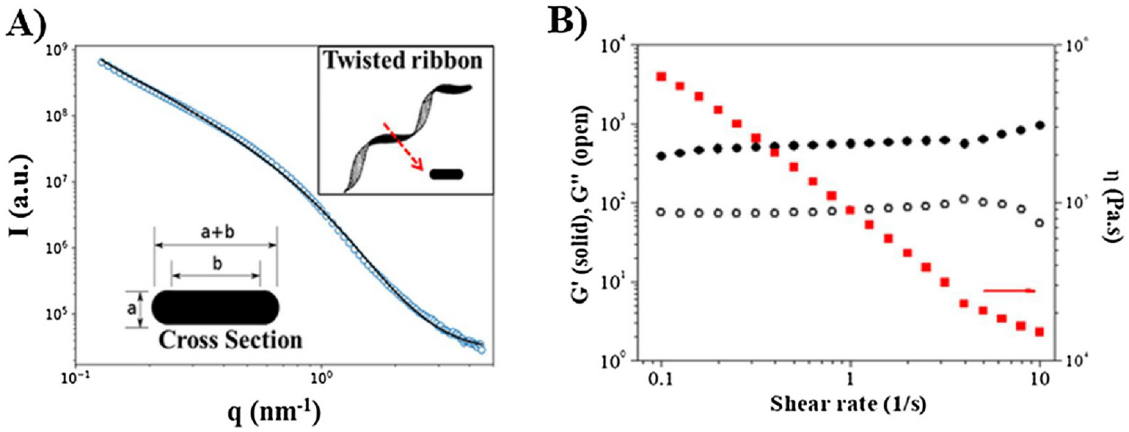

Fig. 3. A) SAXS experimental curve of CNF sample with the corresponding ribbon model fit (-). Scattering intensity(I) as a function of the scattering vector modulus q, in nm^{-1}. The rectangular cross section with semicircle ends of CNF is sketched in the lower left. See the text for details about the model. On the right top, a scheme of CNF as a twisted ribbon with a cross section is drawn. B) Rheological SAOS data obtained for CNF suspensions (1.0 wt%). Viscoelastic G' and G" are presented together with viscosity values (solid squares).

Table 1
Optimized parameters obtained from the SAXS model fitting of Fig. 3 and Rheology from Eq. (1).

Technique	Constants	
SAXS*	**a ± σa (nm)**	**(a + b) ± σa + b (nm)**
	2.6 ± 1.2	46 ± 6
Rheology	**k (Pa s^n)**	**n (a.u.)**
	97090	0.17

*a, σ_a and a + b, σ_{a+b} are the number average and standard deviation of the thickness and overall width of the ribbon's cross section, respectively. Gamma number size distributions are adopted for the *a* and *b* size distributions, as described in the text.

by microscopy are higher than obtained by SAXS, where a model fitting allowed us to obtain two distinct parameters, one for the thickness and other for the width. Furthermore, the accessible q-range didn't allow a meaningful appreciation of the very thick fibers (> 100 nm), which are visible in AFM and TEM images.

Although presented as twisted-ribbon, which increased its assumed diameter, Curauá CNF still present high values of length and a consequent high aspect ratio (L/d). The reduction of particles size after fibers processing causes not only a visual modification of the sample, but also affects bulk properties such as rheological properties. Flexible, CNF may present gel properties with very low mass content (De France et al., 2017). If compared to cellulose nanocrystals, which are rigid, CNFs can reach similar viscosity and present a sol-gel transition in concentrations almost 10 times lower (Benavides, Ao, Davis, & Kitchens, 2011). Here, gel formation was investigated with small-amplitude oscillatory shear (SAOS) rheology, whose results provide rheological information through G' (Storage Modulus) and G" (Viscous Modulus) shown in Fig. 3B. In the gel state G' is much higher than G" (G' > > G"), and a gel can be considered strong (normally formed by crosslinked networks), weak (formed by entangled particles) and intermediary, in case of physical gels. The data in Fig. 3B point to a physical gel, with G' > > G", no cross between storage and loss moduli and a weak dependence on the shear rate. Nanocellulose suspensions are known to present a shear thinning behavior (i.e. a viscosity reduction with frequency increase) owing to the progressive alignment of the fibers along the experiment, which reduces entanglements. The viscosity calculated with Equation 1 decreases with the shear rate, as expected, in Fig. 3B.

$$\eta = k\gamma^{n-1} \quad (1)$$

where viscosity (η) depends on the shear rate (γ) and two constants (k and n), which consistencyand flow behavior index, respectively. Systems with strong shear thinning behavior have n = 0, while for ideal Newtonian fluids n = 1. The parameters used to fit the data (Table 1) are in the same range found before (Nazari et al., 2016) for a strong shear thinning effect. These values are interesting for preparation of injectable materials and can be used to tune experimental conditions for preparation of films.

3.4. Biological response

3.4.1. Cytotoxicity – quantitative and qualitative assay

As described above, the cytotoxicity of nanocellulose materials depends on various parameters and factors, including the source (wood, bacteria, Fique, cotton, Curauá), and extraction process (enzymatic, acid hydrolysis, mechanical process) (Menas et al., 2017). However, the packing of rod-like and twisted-ribbons structure during film preparations can be very different.

Fig. 4A and B shows the images of cells for the negative control (CTL-), positive control (CTL+) and for CNF extract. CTL- maintained cells in a confluent monolayer, whereas for CTL+, there was round and non-adhered cells with the presence of debris. The cells cultured in the presence of CNF extract showed a morphological pattern similar to the CTL-, which cell morphology displays features of fibroblasts, therefore basic cell functions appear not to have suffered alterations due to the contact with CNF extract.

Fig. 4C presents the results of cells viability, where most of the cells were alive for CTL-, representing the 100%. The pattern for the cells grown in the presence of nanofiber extracts was similar to the CTL-, where viable cells around 96 ± 20% were observed (Fig. 4C). The statistical analyses (ANOVA OneWay) showed significant difference ($p < 0.05$) between negative and positive controls (24.6%) and no significant difference between negative control and the cellulose nanofibers. Therefore, based on this cytotoxicity analysis, one should not expect harmful effects from CNF to cells. This conclusion is corroborated by the morphology of the cells in the indirect toxicity test.

In vitro cytotoxicity studies are the first test to check biocompatibility of any material (Freshney, 2005), and the evaluation of mitochondrial activity allows to quantify the viable cells using the MTT assay (Miller & McDevitt, 1991; Wallin & Arscott, 1998). These cytotoxic results are corroborating with the results of Souza et al. (2017) that investigated the CNF toxicity obtained from Fique fibers with similar tests of indirect contact using Vero cells.

3.4.2. Direct contact assay

The cytocompatibility of CNF was evaluated using a direct contact testing assay. This investigation using optical microscopy and SEM techniques are shown in Fig. 5. In addition to CNF films, CTL- with non-cytotoxic behavior and CTL + with cytotoxic effect were also used to measure cytotoxicity effects. In CTL-, cells exhibited efficient proliferation after 24 h, whereas the CTL + showed no cell growth with round morphology typical of non-viable cells.

There is a similar behavior of the cells in the direct tests with the materials relative to the negative control in Fig. 5A, where the cells in contact with the coverslip grew in monolayers and presented an elongated and well spread morphology, characteristic of fibroblast cells. There was little evidence of cell lysis at the negative control similarly to those at CNF tests. On the other hand, for the positive control round, non-adhered cells were observed, in addition to cellular debris. The CNF image in Fig. 5A also point to a cell monolayer like the negative control, although with some differences in the spread morphology. The morphology and basic functions of the cells appear not to be affected by the contact with the materials tested, as it has its characteristic morphology of the fibroblastic-like cells.

The SEM image (Fig. 5B) shows the prolongation of cytoplasm, contours and the cell nucleus, which demonstrates the affinity of Vero cells to CNF films. Such observation is extremely important and means that fibroblast-like cells interact with surface by an initial adhesion process through prolongations of the cells. Furthermore, Fig. 5B indicates cell division marked with a white arrow, which reflects development and cell proliferation onto CNF, while the red arrows mark cytoplasmic prolongations as part of the adherence process.

There is evidence from the literature that cellulose nanofibers obtained from bleached Eucalyptus fibers and Fique fibers are non-toxic (Alexandrescu, Syverud, Gatti, & Chinga-Carrasco, 2013; Souza et al., 2017) and cellulose nanofibers from wood pulp can even be applied as aerogel for drug delivery *in vivo* with good results (Bhandari et al., 2017). However, some unmodified CNF obtained by enzymatic process presented a pro-inflammatory effect (Lopes, Sanchez-Martinez, Strømme, & Ferraz, 2017). In this context, the cell viability of nanocellulose application in biomedicine is dependent of fiber nature, obtainment process, functionalization and mainly desired application. It makes necessary to evaluate the toxicity of these nanoparticles case-by-case.

3.4.3. Adhesion test

The quantification of cells non-adhered on the materials are shown at Fig. 6. The number of cells in the supernatants corresponds to the

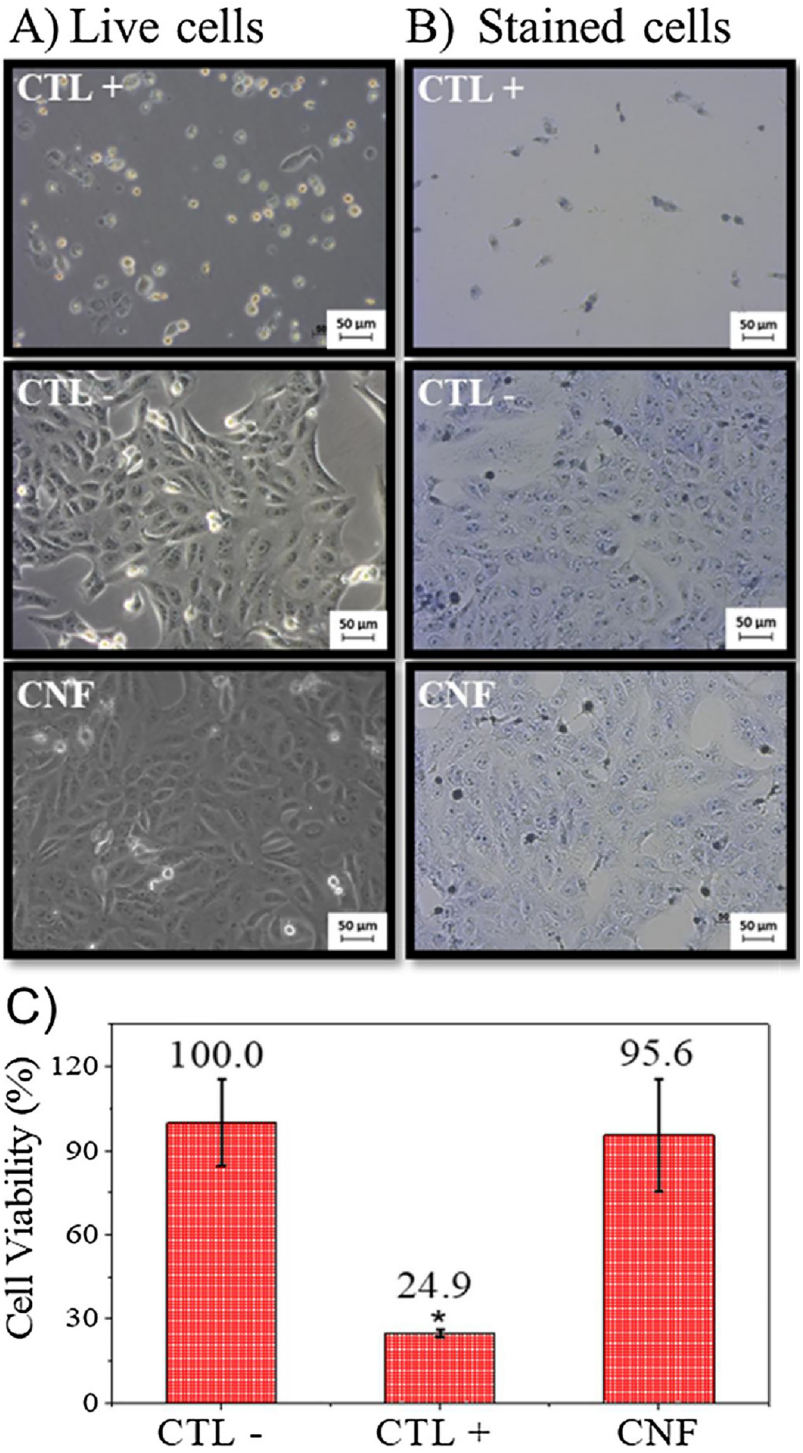

Fig. 4. The photographs show the Vero cells from morphological cytotoxicity assay. A) The live cells are shown on the first column and column B) is presenting the toluidine blue stained cells. C) The cell viability graph from MTT assays. (For interpretation of the references to colour in this figure legend, the reader is referred to the web version of this article.)

non-adhered cells. As expected, CTL- acts as non-adherent substrates and present the higher cell viability (%). CTL + and CNF films had much lower number of cell, being indistinguishable according to the statistical ANOVA analysis using the Tukey test. It reflects the high affinity between the cells and the Curauá cellulosic substrate.

The potential application of nanocellulose materials in different biomedical areas is still in discussion. Steam cells also had great adhesion for CNF hydrogel obtained from sugarcane bagasse (Mertaniemi et al., 2016). Adhesion tests are significant for regenerative tissue and particularly in wound healing fields (Alexandrescu et al., 2013), which indicates that such materials present high potential to be used as scaffold for tissue growing. Therefore, the results of adhesion tests with fibroblast cells reported here for CNF from Curauá are relevant for biomedicine.

4. Conclusions

Along this study, it was possible to obtain nanofibers from Curauá

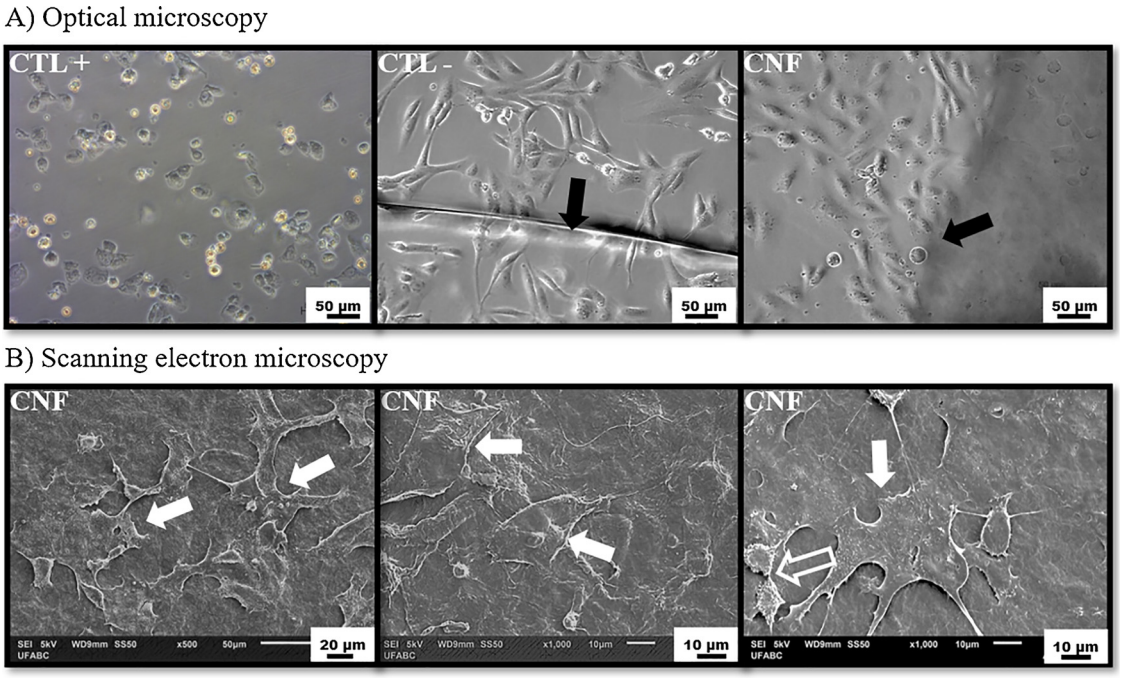

Fig. 5. Morphological analysis from the direct contact assay. A) The optical microscopy images by contrast-phase for CTL+, CTL− and CNF samples. Black arrows indicate the contours plate (coverslip). B) SEM images are showing cells spreading onto the CNF film. The white arrows indicate cells cytoplasmic prolongations, while the empty white arrow is highlighting one cell division.

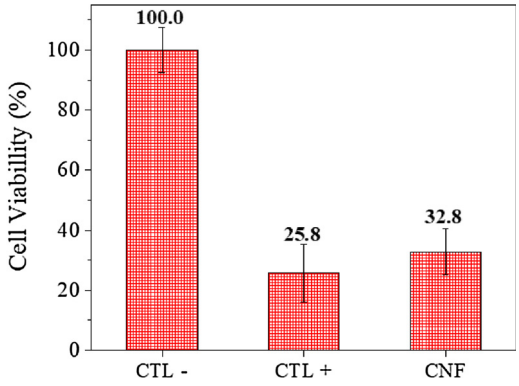

Fig. 6. Adhesion assay results for CTL−, CTL+ and CNF surface.

plant using less chemical and energy consumption in comparison to other natural fibers described in literature. It could be reached due to the high amount of cellulose in the fiber and their intrinsic morphology, consequently, reduced number of cycles into the grinder were used. The obtained nanoparticles showed a ribbon-like morphology that was able to provide an interesting rheological behavior in water. Since these materials show potential applications in biomedicine and pharmacy, several in vitro studies were performed that is necessary since the toxicity of nanocellulose can vary depending on the source, morphology and surface properties. Herein, cellulose nanofibers from Curauá fibers shows no cytotoxicity and good initial biocompatibility for all the tested protocols (direct and indirect test) due to the mild chemical treatments applied to the fibers, which provided nanoparticles with a non-toxic surface and revealed to be an appropriate cellulose source for such applications. Since the cells demonstrated to have great adhesion to its surface, promoting the increasing of cells growing compared to the controls, cellulose nanofibers show potential to be used as scaffolds.

Conflict of interest

The authors declare no competing financial interest.

Acknowledgements

This study was financed by DFAIT (Canada) and CAPES (Brazil) in a Joint Program - Grant Number 7604/13-0. We also thank the Staff at the Centre For Nanostructure Imaging from Department of Chemistry at University of Toronto for the STEM images and LNNano (Brazilian Nanotechnology National Laboratory at CNPEM) for AFM imaging – Proposal AFM-23045.

Appendix A. Supplementary data

Supplementary material related to this article can be found, in the online version, at doi:https://doi.org/10.1016/j.carbpol.2018.08.056.

References

Alexandrescu, L., Syverud, K., Gatti, A., & Chinga-Carrasco, G. (2013). Cytotoxicity tests of cellulose nanofibril-based structures. *Cellulose, 20*(4), 1765–1775.
Bardet, R., Reverdy, C., Belgacem, N., Leirset, I., Syverud, K., Bardet, M., ... Bras, J. (2015). Substitution of nanoclay in high gas barrier films of cellulose nanofibrils with cellulose nanocrystals and thermal treatment. *Cellulose, 22*(2), 1227–1241.
Benavides, E. E. U., Ao, G., Davis, V. A., & Kitchens, C. L. (2011). Rheology and Phase Behavior of Lyotropic Cellulose Nanocrystal Suspensions. *Macromolecules, 44*, 8990–8998.
Bhandari, J., Mishra, H., Mishra, P. K., Wimmer, R., Ahmad, F. J., & Talegaonkar, S. (2017). Cellulose nanofiber aerogel as a promising biomaterial for customized oral drug delivery. *International Journal of Nanomedicine, 12*, 2021–2031.
Castro, D. O., Karim, Z., Medina, L., Haggstrom, J. O., Carosio, F., Svedberg, A., ... Berglund, L. (2018). The use of a pilot-scale continuous paper process for fire retardant cellulose-kaolinite nanocomposites. *Composites Science and Technology* In press.
Charreau, H., Foresti, M. L., & Vazquez, A. (2012). Nanocellulose Patents Trends: A Comprehensive Review on Patents on Cellulose Nanocrystals, Microfibrillated and Bacterial Cellulose. *Recent Patents on Nanotechnology, 7*(1), 56–80.
Cherian, B. M., Leão, A. L., de Souza, S. F., Costa, L. M. M., de Olyveira, G. M., Kottaisamy, M., ... Thomas, S. (2011). Cellulose nanocomposites with nanofibres isolated from pineapple leaf fibers for medical applications. *Carbohydrate Polymers, 86*(4), 1790–1798.
De France, K. J., Hoare, T., & Cranston, E. D. (2017). Review of Hydrogels and Aerogels Containing Nanocellulose. *Chemistry of Materials, 29*, 4609–4631.
Driemeier, C., Pimenta, M. T. B., & Rocha, G. J. M. (2011). Evolution of cellulose crystals during prehydrolysis and soda delignification of sugarcane lignocellulose. *Cellulose,* 1509–1519.

Dufresne, A. (2017). Cellulose nanomaterial reinforced polymer nanocomposites. *Current Opinion in Colloid & Interface Science, 29*, 1–8.
El Baradai, O., Beneventi, D., Alloin, F., Bongiovanni, R., Bruas-Reverdy, N., Bultel, Y., ... Chaussy, D. (2016). Microfibrillated cellulose based ink for eco-sustainable screen printed flexible electrodes in lithium ion batteries. *Journal of Materials Science & Technology, 32*(6), 566–572.
Freshney, R. I. (2005). *). Culture of specific cell types. Culture of animal cells*. Hoboken, NJ, USA: John Wiley & Sons, Inc.
Ghali, L., Msahli, S., Zidi, M., & Sakli, F. (2009). Effect of pre-treatment of Luffa fibres on the structural properties. *Materials Letters, 63*(1), 61–63.
Hoeng, F., Denneulin, A., & Bras, J. (2016). Use of nanocellulose in printed electronics: a review. *Nanoscale, 8*(27), 13131–13154.
Iwamoto, S., Nakagaito, A. N., & Yano, H. (2007). Nano-fibrillation of pulp fibers for the processing of transparent nanocomposites. *Applied Physics A, 89*(2), 461–466.
Jones E., Oliphant T., Peterson P., {SciPy}: Open source scientific tools for {Python}, Retrieved from http://www.citeulike.org/group/19049/article/13344001, 2014.
Jonoobi, M., Oladi, R., Davoudpour, Y., Oksman, K., Dufresne, A., Hamzeh, Y., ... Davoodi, R. (2015). Different preparation methods and properties of nanostructured cellulose from various natural resources and residues: A review. *Cellulose, 22*(2), 935–969.
Jorfi, M., & Foster, E. J. (2015). Recent advances in nanocellulose for biomedical applications. *Journal of Applied Polymer Science, 132*(14), 1–19 9.
Lin, N., & Dufresne, A. (2014). Surface chemistry, morphological analysis and properties of cellulose nanocrystals with gradiented sulfation degrees. *Nanoscale, 6*(10), 5384–5393.
Lopes, V. R., Sanchez-Martinez, C., Strømme, M., & Ferraz, N. (2017). In vitro biological responses to nanofibrillated cellulose by human dermal, lung and immune cells: surface chemistry aspect. *Particle and Fibre Toxicology, 14*, 1 1.
Mao, Y., Liu, K., Zhan, C., Geng, L., Chu, B., & Hsiao, B. S. (2017). Characterization of nanocellulose using small-angle neutron, X-ray, and dynamic light scattering techniques. *The Journal of Physical Chemistry B, 121*(6), 1340–1351.
Mariano, M., Bernardes, S., & Strauss, M. (2018). Mold heat conductance as drive force for tuning freeze-casted nanocellulose foams microarchitecture. *Materials Letters, 225*, 167–170.
Menas, A. L., Yanamala, N., Farcas, M. T., Russo, M., Friend, S., Fournier, P. M., ... Shvedova, A. A. (2017). Fibrillar vs crystalline nanocellulose pulmonary epithelial cell responses: Cytotoxicity or inflammation? *Chemosphere, 171*, 671–680.
Mertaniemi, H., Escobedo-Lucea, C., Sanz-Garcia, A., Gandía, C., Mäkitie, A., Partanen, J., ... Yliperttula, M. (2016). Human stem cell decorated nanocellulose threads for biomedical applications. *Biomaterials, 82*, 208–220.
Miller, R. R., & McDevitt, C. A. (1991). A quantitative microwell assay for chondrocyte cell adhesion. *Analytical Biochemistry, 192*(2), 380–383.
Nazari, B., Kumar, V., Bousfield, D. W., & Toivakka, M. (2016). Rheology of cellulose nanofibers suspensions: Boundary driven flow. *Journal of Rheology, 60*(6), 1151–1159.
Nechyporchuk, O., Belgacem, M. N., & Pignon, F. (2014). Rheological properties of micro-/nanofibrillated cellulose suspensions: wall-slip and shear banding phenomena. *Carbohydrate Polymers, 112*, 432–439.
Nge, T. T., Lee, S.-H., & Endo, T. (2013). Preparation of nanoscale cellulose materials with different morphologies by mechanical treatments and their characterization. *Cellulose, 20*(4), 1841–1852.
Novo, L. P., Bras, J., Garcia, A., Belgacem, M. N., & Curvelo, A. S. (2015). Subcritical water: A method for green production of cellulose nanocrystals. *ACS Sustainable Chemistry & Engineering, 3*, 2839–2846.
Oliveira de Castro, D., Frollini, E., Ruvolo-Filho, A., & Dufresne, A. (2015). "Green polyethylene" and curauá cellulose nanocrystal based nanocomposites: Effect of vegetable oils as coupling agent and processing technique. *Journal of Polymer Science Part B: Polymer Physics, 53*(14), 1010–1019.
Segal, L., Creely, J. J., Martin, A. E., & Conrad, C. M. (1959). An empirical method for estimating the degree of crystallinity of native cellulose using the X-ray diffractometer. *Textile Research Journal, 29*(10), 786–794.
Smyth, M., Fournier, C., Driemeier, C., Picart, C., Foster, E. J., & Bras, J. (2017). Tunable structural and mechanical properties of cellulose nanofiber substrates in aqueous conditions for stem cell culture. *Biomacromolecules, 18*(7), 2034–2044.
Souza, S. F., Leão, A. L., Cai, J. H., Wu, C., Sain, M., & Cherian, B. M. (2010). Nanocellulose from curava fibers and their nanocomposites. *Molecular Crystals and Liquid Crystals, 522*, 42–52.
Souza, S. F., Ferreira, M., Sain, M., Ferreira, M. Z., Pupo, H. F., Cherian, B. M., ... Leão, A. L. (2014). *The use of curauá fibers as reinforcements in compositesBiofiber reinforcements in composite materials* (first ed). Cambridge: Woodhead publishing.
Souza, S. F., Leao, A. L., Lombello, C. B., Sain, M., & Ferreira, M. (2017). Cytotoxicity studies of membranes made with cellulose nanofibers from fique macrofibers. *Journal of Materials Science, 52*(5), 2581–2590.
Su, Y., Burger, C., Hsiao, B. S., Chu, B., & IUCr (2014). Characterization of TEMPO-oxidized cellulose nanofibers in aqueous suspension by small-angle X-ray scattering. *Journal of Applied Crystallography, 47*(2), 788–798.
Wallin, R. F., & Arscott, E. F. (1998). A practical guide to ISO 10993-5: Cytotoxicity. *Medical Device and Diagnostic Industry, 20*, 96–98. Retrieved from https://www.namsa.com/wp-content/uploads/2015/10/A-Practical-Guide-to-ISO-10993-5_-Cytotoxicity.pdf.
Zhao, J., Zhang, W., Zhang, X., Zhang, X., Lu, C., & Deng, Y. (2013). Extraction of cellulose nanofibrils from dry softwood pulp using high shear homogenization. *Carbohydrate Polymers, 97*(2), 695–702.